

Received February 11, 2021, accepted February 19, 2021, date of publication February 24, 2021, date of current version March 4, 2021.

Digital Object Identifier 10.1109/ACCESS.2021.3061647

Probing Packet Retransmission Scheme in Underwater Optical Wireless Communication With Energy Harvesting

CUONG T. NGUYEN¹, VUONG V. MAI², (Member, IEEE), AND CHUYEN T. NGUYEN¹

¹School of Electronics and Telecommunications, Hanoi University of Science and Technology, Hanoi 100000, Vietnam

²School of Electrical Engineering, Korea Advanced Institute of Science and Technology, Daejeon 34141, South Korea

Corresponding author: Chuyen T. Nguyen (chuyen.nguyenthanh@hust.edu.vn)


This work was supported by the Hanoi University of Science and Technology (HUST) under Project T2020-SAHEP-011.

ABSTRACT Underwater Optical Wireless Communication (UOWC) is an up-and-coming technology to support the perception layer of the Internet of Underwater Things (IoUT). However, UOWC channel behaviors can lead to a reduction of IoUT network reliability, while UOWC sensor nodes usually face with the issue of energy limitation. In this paper, we propose a retransmission scheme, which utilizes probing packets and energy harvesting mechanism to solve these issues. The scheme could provide more reliable transmission and energy efficiency for UOWC-based IoUT networks. To investigate the performance of the proposed scheme, we provide an analytical framework based on a two-dimensional Markov chain model. The Monte-Carlo simulation is used to validate the correctness of our analysis. From numerical results, we highlight the advantages of our scheme in comparison with the conventional one. We also determine appropriate values of network parameters to optimize the network performance.

INDEX TERMS Underwater optical wireless communication (UOWC), Internet of Underwater Things (IoUT), automatic repeat request (ARQ), energy harvesting, Markov chain.

I. INTRODUCTION

The internet of underwater things (IoUT), as known as a branch of the internet of things, is defined as a worldwide network of smart interconnected underwater devices with a digital establishment [1]. The applications of IoUT are expected to serve in the field of mine and oil reconnaissance, disaster prevention, environmental monitoring, underwater surveillance, and intrusion detection [2], [3]. To support the concept of IoUT, the underwater wireless sensor networks (UWSNs) have expanded as a part of the perception layer in the IoUT architecture [4]. UWSNs usually include multiple components such as autonomous underwater vehicles (AUVs), observatories, and sensors. They might be deployed in a specific underwater area to perform real-time monitoring and record high-resolution images and videos. To achieve these tasks, a wireless communication solution with high data-rate transmission and low latency is required [5].

The associate editor coordinating the review of this manuscript and approving it for publication was Tao Wang .

Several approaches have been investigated to meet the requirement of the underwater environment. On one hand, traditional acoustic communication has stimulated many research works thanks to its low path-loss and long communication range. However, its performance is restricted by narrow bandwidth, high delay, and time-varying multi-path propagation [6], [7]. Radio-frequency (RF) is also recommended as it offers high data rate transfer. The RF communication, nevertheless, requires high transmitted power in freshwater while the transmitted signal is attenuated rapidly in seawater, which make it incompatible with UWSN applications [8], [9]. On the other hand, underwater optical wireless communication (UOWC) has emerged as another promising candidate for the deployment of future UWSNs. It has been proved that for a short-range transmission, UOWC can provide much higher data rates with significantly lower power depletion and effortless computational algorithms in comparison with the aforementioned communication technologies [9].

Despite the advantages, UOWC sensor networks face with several challenging issues. Firstly, the propagation of

light is severely suffered by various underwater phenomena. Comprehensive studies have pointed out three main degrading factors, i.e., absorption, scattering, and turbulence-induced fading. Secondly, interference power and different noise sources should also be taken into account when studying the optical channel's precision in certain circumstances. The energy limitation of sensor nodes in UWSNs is the final major problem. This limitation restricts a sensor node's transmitted power and thus, reduces its coverage distance and reliability. Moreover, replacing or recharging the battery for each node is also very challenging. The node can deal with this problem by using a large battery, with the trade-off between mobility and cost [10].

The first two issues can adversely affect the reliability of UOWC-based IoUT networks. In this situation, error correction techniques i.e., forward error correction (FEC) and automatic repeat request (ARQ) could improve the network performance. In FEC, some controlled bits are added to the transmitted packets for the recovery when they are in error at a limited number of bits [11], [12]. In ARQ, the retransmission of failed packets is used for error correction. Compared with ARQ, FEC requires more complex computational capability. Also, the ARQ overhead is lower than that of FEC in the good channel condition due to no frequent retransmissions and redundancy needed. There have been several studies of ARQ in UOWC. For example, ARQ and single-photon avalanche (SPAD) detectors were utilized to mitigate different underwater impairments, thus increasing the coverage of UOWC networks [13]. In [14], an ARQ application in improving the performance of medium access control (MAC) was studied. The current studies have directly applied conventional ARQ schemes into UOWC contexts. However, since retransmissions certainly result in more energy consumption, the conventional ARQ without modifications may not perform effectively under the energy limitation of UOWC nodes.

On the other hand, energy harvesting has been advocated as one of the most promising solutions for the energy issue in general wireless networks [15]. For UOWC, there were several works on energy harvesting. A study in [16] considered an energy-harvesting UOWC sensor network where nodes can harvest and store ambient renewable energy sources. Another study in [17] proposed a UWSN using hybrid RF/optical communications and optical energy harvesting. These studies have concluded that energy harvesting can jointly work with other techniques, e.g., localization [16] and media diversity [17], to improve overall network performance.

From the above analysis, we can see that reliability and energy are the two most crucial issues in UOWC networks. Also, an amalgamation of retransmission (with probing packets) and energy harvesting could potentially solve both the reliability and energy issues. However, this amalgamation has never been investigated in the past. The contributions of our paper are summarized as follows:

- 1) We propose a retransmission scheme, namely ARQ-PE, for UOWC-based IoUT networks. ARQ-PE uses an additional probing packet (in a basic energy level) to predict the channel condition before deciding whether to transmit a data packet (in a higher energy level). Also, energy harvesting is activated as a part of the ARQ-PE operation. Therefore, ARQ-PE could improve the successful transmission rate and also use energy more effectively.
- 2) To investigate the performance of the proposed ARQ-PE, we propose an analytical framework based on a two-dimensional (2-D) Markov chain model. This model allows us to analyze the crucial network performance metrics, including throughput, delay, and energy efficiency. Our performance analysis also considers various physical layer impairments on UOWC channels, such as absorption, scattering, turbulence-induced fading, interference, and receiver noise. The Monte-Carlo simulations are used to validate the correctness of our proposed analysis.
- 3) Based on the analytical framework, we compare the performance of ARQ-PE and the conventional ARQ to highlight the advantages of ARQ-PE. The appropriate values of some parameters, e.g., number of nodes and transmission power, are determined for the network design. We also investigate the optimal number of retransmissions to maximize throughput and reduce the delay.

The rest of the paper is organized as follows. In Section II, we review our network model. Section III presents the proposed ARQ-PE and its performance analysis. In Section IV, the analytical results are validated by simulation, and numerical results are presented. Finally, Section V concludes the paper.

II. NETWORK MODEL

In this section, our considered network model is described, in which the bit-error-rate (BER) performance is analyzed under the effect of various physical factors on the optical signal, i.e., water type, turbulence fading, noise, and interference.

A. NETWORK DESCRIPTION

Fig. 1 depicts a UOWC-based IoUT network model, which includes an omnidirectional optical access point (OAP) [18] and sensor nodes. The OAP is indicated by a gray star at the center of a 3-dimensional communication area specified by a radius of R meters. A square and circles, respectively, represent the desired signal node and n interference nodes. It should be noted that n interference nodes are assumed to be uniformly distributed in the 3-D area. The distance between the OAP and the desired signal node is d meters. The OAP tries to gather information from the desired signal node through a point-to-point underwater optical wireless channel in the considered situation. The channel is affected by the interference signal from n other nodes and various

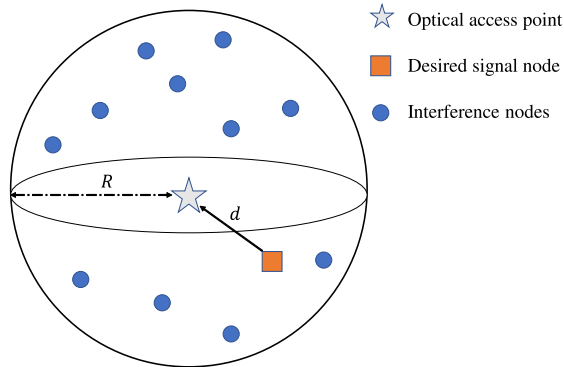


FIGURE 1. A 3-D model of underwater optical wireless sensor network.

environmental factors such as water types and turbulence fading characteristics.

We study the network in a time-division-multiple-access mode where a time slot is defined as a necessary time that the desired node completes the transmission of one packet. In each time slot, the desired sensor node can do two independent actions: harvesting energy and transmitting a packet. Although the harvested energy from multiple sources might be practically unstable, in this article, we assume that the node harvests energy constantly at the rate of E_{hv} energy units per time slot for simplicity. For the packet transmission, we denote by E_{tx}^d the energy units required to transmit a data packet. Moreover, the packet arrival is assumed following a Poisson process with an average arrival rate of λ_{packet} (packets/time slot). If a packet is received successfully by the OAP, an active acknowledgment (ACK) is responded to the node, while a negative acknowledgment (NAK) is used, otherwise.

To supply and store energy, the desired node is equipped with a battery that has a maximum value of E_{max} energy units. The energy level of the battery depends on the process of harvesting and consuming energy of the sensor node. For example, let say $E_c(t)$ and $E_h(t)$ are the energy consumption and the energy harvesting of the sensor node in t^{th} time slot, respectively. If $E_c(t) > E_h(t)$, the battery loses its energy power. On the contrary, if $E_c(t) < E_h(t)$, the redundant energy will be stored in the battery. Here, a multi-harvester architecture [19] can be employed for the node so that it can harvest energy from different sources such as microbial fuel cells (MFCs), sunlight, or water flow. It is shown in [20] that the MFCs can provide up to 6 Watt per meter square, which is sufficient to power and maintain the sensor node. It is noted that the current energy level of the sensor nodes can be determined by several energy estimation algorithms as shown in [21]. Furthermore, the considered node has two modes, i.e., active and sleep, based on its current energy level. In particular, a node is at sleep mode when its energy level is below a threshold of E_{th} energy units, and in this case, the node drops out any current data packets and denies all arriving packets. The desired node operates the packet transmission normally at the active mode, where the energy level is higher than E_{th} energy units.

B. SIGNAL-TO-INTERFERENCE-PLUS-NOISE RATIO

The signal-to-interference-plus-noise ratio (SINR) is defined as the received signal power at the OAP from the desired node divided by the sum of the interference power and the power of noise. We denote by S , I , and N the desired signal, interference, and noise components, respectively.

1) DESIRED SIGNAL

The desired signal S is given by [22]

$$S = \gamma^2 (P_{r,s})^2, \quad (1)$$

in which γ is the optical-to-electrical (O/E) conversion efficiency. $P_{r,s}$ is the optical received power from desired signal node, which is written as [23]

$$P_{r,s} = P_t \delta_t \delta_r e^{-c(\lambda)d} \frac{A_r}{2\pi d^2}, \quad (2)$$

where P_t is the optical transmitted power; δ_t and δ_r are respectively the transmitter and receiver optical efficiency; A_r is the receiver aperture area; $c(\lambda)$ is the extinction coefficient, that can be computed as

$$c(\lambda) = a(\lambda) + b(\lambda), \quad (3)$$

where $a(\lambda)$ and $b(\lambda)$ represent the absorption and scattering coefficient respectively. The detailed formula for these coefficients can be found in [24].

2) INTERFERENCE SIGNAL AND NOISE

The interference signal I from n interference nodes is computed as

$$I = \gamma^2 \left(\sum_{i=1}^n P_{r,i} \right)^2 = \gamma^2 \left(\sum_{i=1}^n P_t \delta_t \delta_r e^{-c(\lambda)d_i} \frac{A_r}{2\pi d_i^2} \right)^2, \quad (4)$$

in which $P_{r,i}$ is the optical received power from i -th interference node; d_i is the distance between i -th interference node and the OAP. We call X as a random variable which represents the distance from each interference nodes to the OAP or $X = \{d_i | i = 1, \dots, n\}$. As mentioned above, all n interference nodes are uniformly distributed within the network area in Fig. 1. Thus, according to [25], the probability density function of X , denoted as $f_X(x)$, is expressed as follows

$$f_X(x) = \begin{cases} \frac{3x^2}{R^3} & 0 < x < R \\ 0 & \text{otherwise.} \end{cases} \quad (5)$$

Due to the randomness of X , the interference component is derived in an average method. Let Y is a random variable and a function of X , which $Y = \frac{e^{-c(\lambda)X}}{X^2}$. We first find the expected value of Y calculated as [26]

$$\begin{aligned} E[Y] &= \int_0^R \frac{e^{-c(\lambda)x}}{x^2} \frac{3x^2}{R^3} dx \\ &= \frac{3}{c(\lambda)R^3} \left(1 - e^{-c(\lambda)R} \right). \end{aligned} \quad (6)$$

Then, the expected value of the received power from all n interference nodes is expressed as

$$E \left[\sum_{i=1}^n P_{r,i} \right] = n P_t \delta_r \delta_r \frac{A_r}{2\pi} \frac{3}{c(\lambda)R^3} \left(1 - e^{-c(\lambda)R} \right). \quad (7)$$

On the other hand, the noise component N , including thermal noise and shot noise, is given by [22]

$$N = \sigma_{\text{shot}}^2 + \sigma_{\text{thermal}}^2, \quad (8)$$

where σ_{shot}^2 and $\sigma_{\text{thermal}}^2$, respectively, denote by the variances of the shot noise and the thermal noise. Note that, both the noises are modeled as Gaussian processes with zero-mean. The SINR in our network model can be finally calculated [27],

$$\text{SINR} = \frac{Sf(c(\lambda), n)}{I + N}, \quad (9)$$

where S , I , and N can be respectively found at (1), (4), and (8); $f(c(\lambda), n)$ is a coefficient function added to the numerator of (9) to improve the accuracy of the approximated SINR. A matching method is used in [27] to form the $f(c(\lambda), n)$, which can be numerically found as follows

$$f(c(\lambda), n) = 1 - ne^{-c(\lambda)-4}. \quad (10)$$

Moreover, the same method can also be used to determine similar forms of $f(c(\lambda), n)$ for different network setups.

C. BIT-ERROR-RATE

Next, we study the bit-error-rate (BER) behavior in UOWC networks using the above investigation of the SINR. As [28], under the effects of the turbulence fading, the UOWC fluctuation might follow the exponentiated Weibull (EW) distribution. The probability density function of EW distribution, $f_h(h)$, is obtained as

$$f_h(h) = \frac{\alpha\beta}{\eta} \left(\frac{h}{\eta} \right)^{\beta-1} \exp \left[- \left(\frac{h}{\eta} \right)^\beta \right] \times \left\{ 1 - \exp \left[- \left(\frac{h}{\eta} \right)^\beta \right] \right\}^{\alpha-1}, \quad (11)$$

where h denotes by the irradiance of optical wave; α, β are shape parameters; η is the scale parameter ($\alpha, \beta, \eta, h > 0$). The expression of the distribution parameters is approximately computed as [29]

$$\alpha \simeq \frac{7.22\sigma_I^{2/3}}{\Gamma(2.487\sigma_I^{2/3} - 0.104)}, \quad (12a)$$

$$\beta \simeq 1.012 \left(\alpha\sigma_I^2 \right)^{-13/25} + 0.142, \quad (12b)$$

$$\eta = \frac{1}{\alpha\Gamma(1 + 1/\beta) g_1(\alpha, \beta)}, \quad (12c)$$

$$\text{with } g_1(\alpha, \beta) = \sum_{j=0}^{\infty} \frac{(-1)^j \Gamma(\alpha)}{j! (j+1)^{1+\frac{1}{\beta}} \Gamma(\alpha-j)}, \quad (12d)$$

where Γ is the Gamma function and σ_I^2 is the scintillation index. Then, by assuming on/off keying (OOK) modulation for simplicity, the BER formula is given by

$$\begin{aligned} \text{BER} &= \frac{1}{2} \int_0^\infty \text{erfc} \left(\frac{\text{SINR}h}{2\sqrt{2}} \right) f_h(h) dh \\ &= \frac{\alpha\beta\sqrt{v\pi}}{2\sigma(2\pi)^{\frac{u+v}{2}}} \left(\frac{u}{\sigma} \right)^{\frac{\beta}{2}-1} \sum_{j=0}^{\infty} \frac{(-1)^j \Gamma(\alpha)}{j! \Gamma(\alpha-j)} \\ &\quad \times G_{2u, v+u}^{v, 2u} \left[\left(\frac{\omega_j}{v} \right)^v \left(\frac{u}{\sigma} \right)^u \middle| \begin{matrix} \Delta(u, 1-\frac{\beta}{2}), \Delta(u, \frac{1}{2}-\frac{\beta}{2}) \\ \Delta(v, 0), \Delta(u, -\frac{\beta}{2}) \end{matrix} \right], \end{aligned} \quad (13)$$

where $\text{erfc}(z)$ is the complementary error function of z ; $\omega_j = j + 1$; $\sigma = \frac{(\eta\text{SINR})^2}{8}$; u and v are integers that satisfy $\frac{u}{v} = \frac{\beta}{2}$; $\Delta(k, a)$ is a series of $\frac{a}{k}, \frac{a+1}{k}, \dots, \frac{a+k-1}{k}$; $G_{p,q}^{m,n}[\cdot]$ is known as the Meijer's G-function. Although Eq. (13) is given in terms of an infinite summation, usually about 30 terms are needed for the series to converge.

III. PROPOSED RETRANSMISSION SCHEME

In this section, a detailed description of the proposed automatic repeat request with probing (ARQ-PE) protocol is presented. Based on the protocol, the performance of network throughput and energy efficiency is analyzed by considering the Markov chain model of state transition of ARQ-PE. The network delay will also be investigated.

A. PROTOCOL DESCRIPTION

The proposed ARQ-PE scheme is based on the stop-and-wait ARQ combining with the probing technique and energy harvesting, while it can be applied for other retransmission schemes without loss of generality. The scheme will be performed sequentially according to the following steps during each time slot. Firstly, the desired node having a data packet checks if it is currently in the active mode (its energy level is greater than E_{th} energy units). If it is not, the current data packet is dropped out, and the node turns into sleep mode. More specifically, the desired node will start the transmission in each time slot by sending a probing packet to detect the channel condition. The receiver, or the OAP in this situation, after obtaining the probing packet, will check the received power level and compare it with a predefined threshold. If the level is greater (or smaller) than the threshold, the ACK (or the NAK) is transmitted back. Moreover, the energy required to transmit a probing packet is independent of the energy required to transmit a data packet E_{tx}^d , and we denoted it as E_{tx}^p .

The considered node depending on the feedback of the probing packet, i.e., ACK or NAK, determines the subsequent actions. We assume that the channel is unchanged during each time slot, in which the data and probing packets are both transmitted. This implies that the data packet will be transmitted successfully if the ACK of the probing packet is received. However, if NAK feedback is received, the data packet transmission is postponed to the next time slot.

The desired node will continually transmit the data packet in the following time slots until the transmission is successful, or a number of retransmissions reaches a maximum threshold, which is denoted by K . A schematic diagram of the proposed ARQ-PE mechanism is shown in Fig. 2. It is noted that the sensor keeps harvesting energy synchronously throughout the whole process, while the considered harvesting rate includes both the actual one and the discharge one.

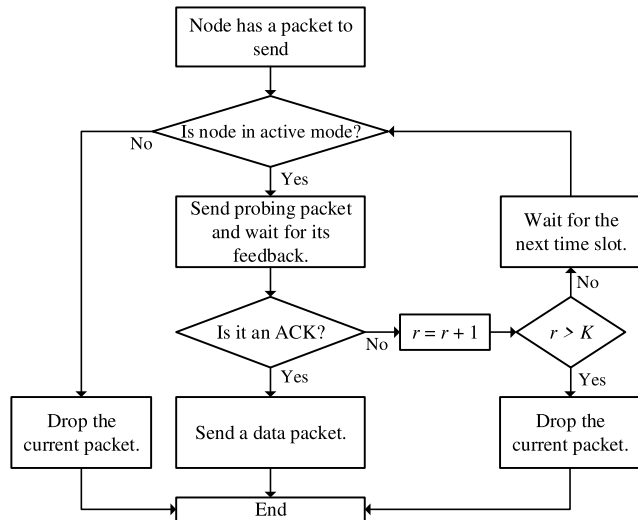


FIGURE 2. Packet transmission of desired node with the proposed ARQ-PE protocol (r is the retransmission counter initially set by 0).

There is one thing that should be mindful of the threshold E_{th} is that $E_{th} > E_{tx}^d + E_{tx}^p$. Once the sensor node enters active mode, it is necessary to ensure that the desired node has enough energy to complete a transmission fully. In the case of ARQ-PE, it is the energy required to transmit a data packet and a probing packet. Suppose the desired node transmits a probing packet successfully, but its remaining energy is not enough to send the follow-up data packet. In that case, the node will have to wait until the energy is harvested enough. In that situation, the probing packet will become useless because the channel condition may change at that time. So, the setting of E_{th} is important for ARQ-PE to operate correctly.

Moreover, the forward error control (FEC) algorithm is also added up to improve the error control performance. We assume that all data packets have a length of L bits and FEC help to detect and correct up to ℓ_b erroneous bits. Therefore, the frame error rate, in this case, is defined as the probability that there are more than ℓ_b bit-errors in one data packet or can be expressed as follows

$$FER = 1 - \sum_{p=0}^{\ell_b} \binom{L}{p} BER^p (1 - BER)^{L-p}. \quad (14)$$

B. THROUGHPUT AND ENERGY EFFICIENCY

We analyze the proposed ARQ-PE protocol's network throughput and energy efficiency performance by

considering the Markov chain model of state transition. The throughput is defined as the number of successfully transmitted bits over a period of time and can be computed as

$$Thp = P_{succ} R_b, \quad (15)$$

in which R_b is the data bit rate, and P_{succ} is the average probability that a packet is transmitted successfully during a time slot. Energy efficiency is also an important designing aspect in the UOWC-based IoUT network. The energy efficiency η_{EE} , interpreted as the number of successfully transmitted bits per joule, is determined as

$$\eta_{EE} = \frac{Thp}{P_t}. \quad (16)$$

It is noted here that the transmission power P_t will affect the energy consumed for a data packer transmission E_{tx}^d . Because if the P_t increases, the signal energy associated with each data bit will enlarge and, thus, the cost of a data packet E_{tx}^d goes up. For the simplicity of the relationship between two dimensions, we have 1 joule = 10^5 energy units. As a result, we represent the E_{tx}^d as follows

$$E_{tx}^d = \frac{P_t L}{R_b}. \quad (17)$$

This is similar to $E_{tx}^d = 100$ energy units when $P_t = 10$ (W).

To obtain the probability P_{succ} , we analyze the behavior of the sensor node. By considering the energy harvesting-consumption process, the performance of the packet transmission of the desired node is modeled via a finite-state Markov chain, which is depicted in Fig. 3. The figure is divided into two sub-figures: Fig. 3a describes the general state transition of ARQ-PE including two modes, i.e., sleep and active; Fig. 3b describes the state transition in the active mode in detail. We assume here that the total number of states is m . Additionally, each state i ($0 < i \leq m$) in the Markov chain model is uniquely represented by two variables, namely $\{S_r^i, S_e^i\}$, in which S_r^i and S_e^i , respectively, denote by the number of retransmissions and the energy level of the sensor for a given time slot.

Each type of line in Fig. 3 depicts different processes: the solid lines define the process of harvesting energy only with the gain of E_{hv} energy units; the dashed lines define the process, in which the node fails to transmit a data packet and send a probing packet only. The energy lost due to this process is denoted as E_F , which can be express as $E_F = E_{tx}^p - E_{hv}$; The dash-dotted lines define the process of sending a data packet successfully, which means the energy lost in this case, E_S , can be written as $E_S = E_{tx}^d + E_{tx}^p - E_{hv}$. It is important to note that $E_{tx}^p > E_{hv}$. Moreover, E_0 is the initial energy level and $E_{pp} = E_{max} - KE_F$. The threshold energy level E_{th} is computed as $E_{th} = E_0 + E_S$. Owing to the normalization of the energy harvesting processes, E_{max} , E_0 , E_{hv} , E_{th} , E_{tx}^d , E_{tx}^p , E_F , E_S , E_{pp} are all integers.

The probability P_{succ} is computed as follows

$$P_{succ} = \sum_{i=0}^m \pi_i P_g(i) (1 - FER), \quad (18)$$

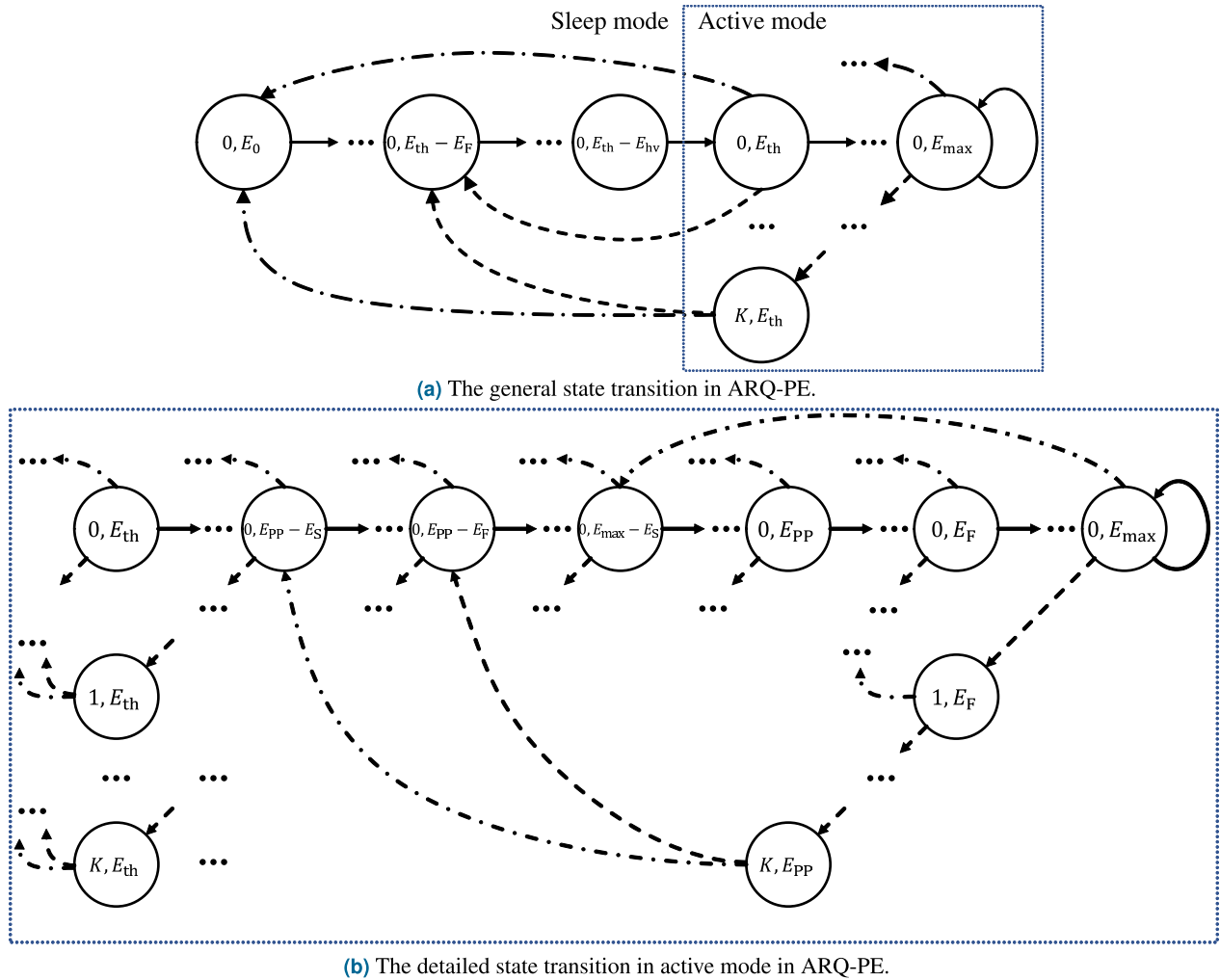


FIGURE 3. Markov chain model of state transition for ARQ-PE.

where π_i is a stationary probability that the node is currently in state i and can be obtained from the Markov chain model; $P_g(i)$ is a probability that the node in state i has a packet to transmit, which is expressed as follows

$$P_g(i) = \begin{cases} 1 - e^{-\lambda_{\text{packet}}}, & S_r^i = 0 \\ 1, & S_r^i \neq 0 \\ 0, & E_0 \leq S_e^i < E_{th} \end{cases}, \quad \begin{matrix} E_{th} \leq S_e^i \leq E_{max} \\ E_0 \leq S_e^i < E_{th} \end{matrix} \quad (19)$$

We are now going to find the stationary probability vector $\pi = [\pi_1, \dots, \pi_m]$. In particular, according to Markov theory [30], we have

$$\begin{cases} \pi \cdot Q = \pi \\ \sum_{i=1}^m \pi_i = 1, \end{cases} \quad (20)$$

where Q is a $m \times m$ transition probability matrix. In other words, Q_{ij} denotes by a probability that the node, which is

currently in state i , will be in state j at the next time slot. It can be found as follows

- 1) If the node has no packet, it only harvests the energy (E_{hv} energy units) during a time slot, and thus

$$Q_{\{0, S_e^j\} \{0, S_e^i + E_{hv}\}} = 1 - P_g(i), \quad (21)$$

in which $S_e^i < E_{max}$. Here, it is noted that if the energy level is detected to be maximum, the node will stop the harvesting process. The energy level will be unchanged without transmission, or

$$Q_{\{0, E_{max}\} \{0, E_{max}\}} = 1 - P_g(i). \quad (22)$$

- 2) If the node has a packet to send, it transmits a probing packet only if $E_{th} \leq S_e^i \leq E_{max}$. If the transmission is successful, the data packet will be also received correctly. In this case, the retransmission counter is reset by 0, while the energy level is reduced by E_S energy units, as follows

$$Q_{\{S_r^i, S_e^j\} \{0, S_e^i - E_S\}} = P_g(i) (1 - FER). \quad (23)$$

- 3) In case the probing packet transmission is unsuccessful, the energy is consumed by E_F energy units. The node will try to retransmit the packet at the next time slot when $E_{th} + E_F \leq S_e^i \leq E_{max}$. As a result, we have

$$Q_{\{S_r^i, S_e^i\} \{S_r^{i+1}, S_e^i - E_F\}} = P_g(i) FER. \quad (24)$$

However, if $E_{th} \leq S_e^i < E_{th} + E_F$, the node drops the current packet and puts itself into the sleep mode, and we expressed as

$$Q_{\{S_r^i, S_e^i\} \{0, S_e^i - E_F\}} = P_g(i) FER. \quad (25)$$

It is noted here that in these situations, the retransmission counter has not reached the maximum number or $S_r^i < K$.

- 4) When the node reaches the maximum number of retransmission while the transmission of the probing packet is still unsuccessful, it also drops the packet, i.e.,

$$Q_{\{K, S_e^i\} \{0, S_e^i - E_F\}} = FER, \quad (26)$$

where $E_{th} \leq S_e^i \leq E_{pp}$. In the other cases, $Q_{ij} = 0$. The throughput and energy efficiency can now be derived from (15), (16), (20), and (23).

C. DELAY

We investigate the network delay, which is defined as the average total delay the node takes to transmit a data packet successfully. In a given time slot, there are three possible scenarios as follows. Firstly, the node has no data packet and only harvests energy; secondly, the node transmits a probing packet, and the transmission is unsuccessful; finally, the transmission of the probing packet is successful, and the follow-up data packet is sent. Each event causes a different delay to the network, and we respectively denote the delays of the first, second, and final event as D_1 , D_2 , and D_3 . Therefore, the network delay D is expressed as follows

$$D = D_1 P(D_1) + D_2 P(D_2) + D_3 P(D_3), \quad (27)$$

where $P(D_1)$, $P(D_2)$ and $P(D_3)$ are the probability that the first, second and final events happen in a given time slot respectively. In this article, we assume that $D_1 = 0$ because harvesting energy causes no delay to the network. Accordingly, only the second and final events should be noticed in (27). The probability of the unsuccessful transmission, $P(D_2)$, can be written as

$$P(D_2) = \sum_{i=0}^m \pi_i P_g(i) FER. \quad (28)$$

The probability of the successful transmission, $P(D_3)$, is computed as

$$P(D_3) = \sum_{i=0}^m \pi_i P_g(i) (1 - FER). \quad (29)$$

IV. NUMERICAL RESULTS AND DISCUSSION

In this section, we investigate the performance of conventional ARQ and ARQ-PE through the above aspects, including the throughput, the delay, and the energy efficiency, with different parameters setup. The conventional ARQ is understood as the retransmission scheme without the probing technique. The performance of conventional ARQ can be obtained by simplifying the proposed analysis of ARQ-PE. MATLAB-based simulation results are used to validate the analytical results and are numerically evaluated by the Monte-Carlo method, with an average of 10^6 time slots. The pure seawater, whose extinction coefficient $c(\lambda)$ is 0.056, is used throughout the results. The characteristics of the Exponentiated Weibull are chosen as $\alpha = 7.3$, $\beta = 7.94$, $\eta = 0.91$ from [28]. Without further notice, the number of retransmissions, K , is set to be 2, the communication distance, d , is 10 (m), the transmit power, P_t , is 10 (W) (the high transmit power is practically feasible by using an LED array [31]), and the number of interference nodes, n , is 20. Other parameters can be found in Table 1.

TABLE 1. Parameters used in simulation.

Parameters	Symbol	Value
Data bit rate	R_b	1.28 (Mbps)
Noise bandwidth	B	100 (MHz)
Network size	R	500 (m)
The receiver optical efficiency	δ_r	0.9
The transmitter optical efficiency	δ_t	0.9
O/E conversion efficiency	γ	0.54
The receiver aperture area	A_r	0.01
The electron charge	q	1.6×10^{-19} (C)
Absolute temperature	T_k	298 ($^{\circ}K$)
Boltzmann's constant	k	1.38×10^{-23} (J/K)
Noise bandwidth factor	I_2	0.562
Open-loop voltage gain	G	10
The FET channel noise factor	Γ_n	1.5
The FET trans-conductance	g_m	30×10^{-3}
PD capacitance per unit area	η_p	112×10^{-8}
Background current	I_{bg}	5100 (μA)
Frame length	L	128 bits
FEC parameter	l_b	6 bits
Initial energy level	E_0	1 energy unit
Battery maximum capacity	E_{max}	800 energy units
Energy harvest rate	E_{hv}^p	10 energy units
Energy consumption for a probing packet	E_{tx}^p	20 energy units
Packet arrival rate	λ_{packet}	0.1
The delay for second event	D_2	20 (ms)
The delay for final event	D_3	120 (ms)

A. THROUGHPUT

Firstly, in Fig. 4, we show the impact of the energy harvesting scheme on the performance of both the conventional ARQ and the proposed ARQ-PE. All parameters are set by default and all protocols are simulated in the same period of time. The desired node without EH is equipped with a battery that has a maximum capacity of 10 times larger than that of the battery used in the systems with EH. It is seen from the figure that the protocols with EH perform better than those without EH when the packet rate is increased. This is because protocols without EH may only handle a fixed

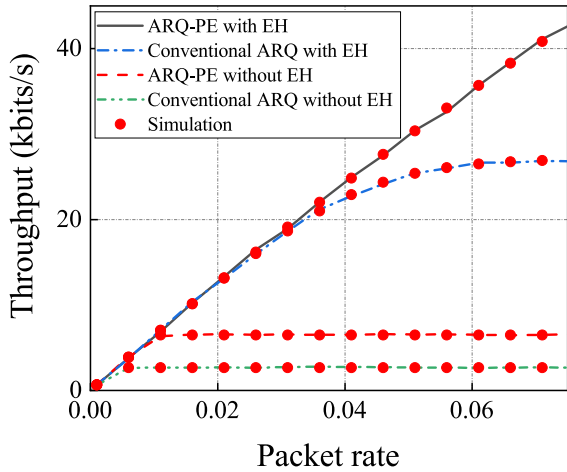


FIGURE 4. Performance comparison of protocols with and without energy harvesting.

number of transmissions in a fixed period due to the limited capacity. It confirms the important role of energy harvesting schemes in IoT applications. Therefore, we mainly focus on the performance of conventional ARQ and ARQ-PE with EH. Besides, it is seen from the figure that the analytical results are perfectly matched with the simulation ones, which validates our above analysis.

We plot in Fig. 5 the throughput versus the distance between the desired node and the OAP. It is seen that the throughput performance of ARQ-PE is better than that of conventional ARQ when the distance $d > 9.6$ meters. It happens because the ARQ-PE technique helps to save energy and keep the node active more frequently when the BER is high. Note that the useful range is limited ($d < 10.5$ meters), and it is crucial for locating the right position to achieve the desired performance. For a smaller transmission distance ($d < 9.6$ meters, in this case) when the communication channel becomes better, the use of the probing

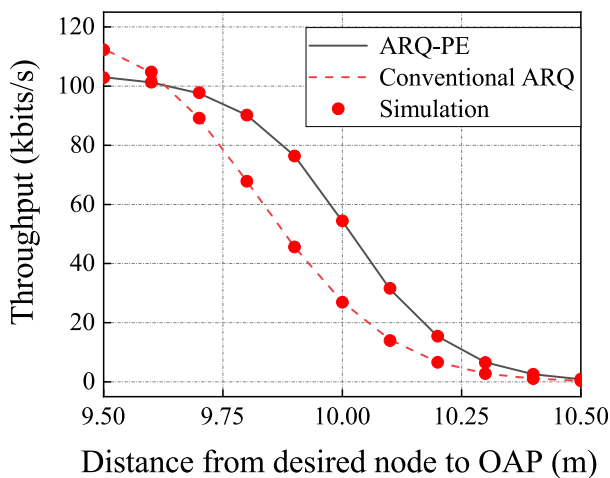


FIGURE 5. Throughput versus distance between the desired node and the OAP for conventional ARQ and ARQ-PE.

packet might take more time for a successful data packet transmission in comparison with the conventional ARQ. As a result, the obtained throughput might be lower than that of the conventional ARQ.

Fig. 6 represents the throughput of ARQ-PE with different numbers of retransmissions with the same settings as in Fig. 5. The retransmissions create more chances for a packet to transmit successfully. It explains why the throughput is increased as well as the number of retransmissions. Another noticed thing is that when the communication distance reaches 10 meters, the increase in throughput decreases gradually as K goes up. And when $K \geq 3$, the throughput is nearly saturated with the value of nearly 60 kbps. It can be explained by the limitation of energy capacity, which restricts the node to transmit only with a finite number of transmissions. Therefore, setting the number of retransmission K to optimize the performance is necessary when deploying in particular network setups.

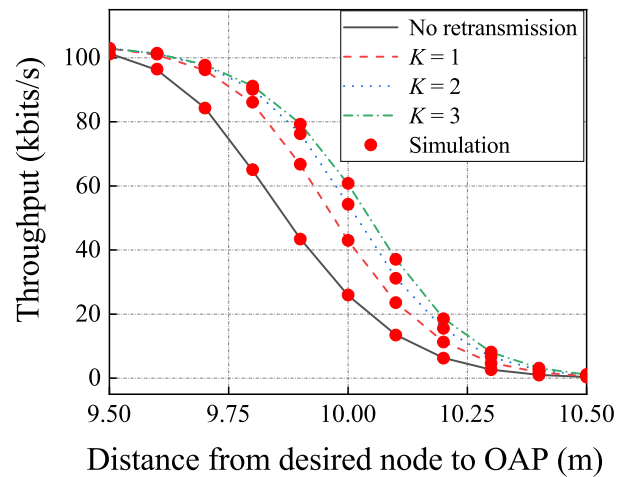


FIGURE 6. Throughput versus distance between the desired node and the OAP for ARQ-PE with different numbers of K .

Fig. 7 plots the throughput with respect to the number of interference nodes for ARQ-PE and conventional ARQ. The conventional ARQ shows a good throughput as the number of interference nodes is insignificant or $n < 10$, particularly. On the other hand, the throughput performance of ARQ-PE is better when the interference component increases, which is $n > 10$. With a growing demand for digital underwater devices, there will be more interference sources appearing densely in the area of UWSNs. Hence, ARQ-PE is a suitable approach in the future of IoUT.

Next, the throughput of ARQ-PE with different K in the aspect of the number of interference nodes is shown in Fig. 8. As we see, the reduction in the network throughput, which is due to the interference power, can be enhanced by the number of retransmissions. In particular, the gap between $K = 3$ case and no retransmission case is significantly considerable. However, when the network is less dense ($n < 10$) or more dense ($n > 35$), there is no difference at all. Accordingly, an optimal selection of K can be derived from the results

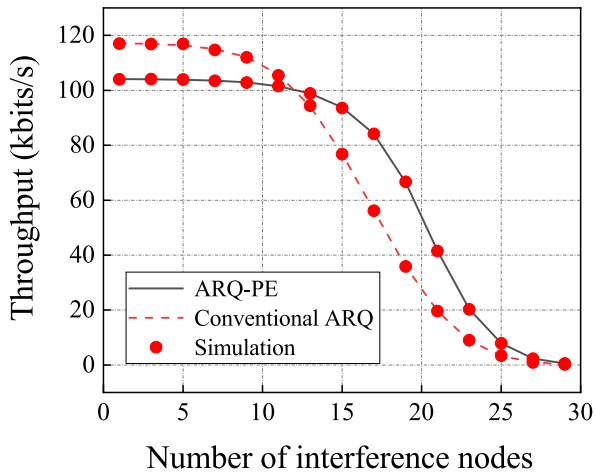


FIGURE 7. Throughput versus the number of interference nodes for conventional ARQ and ARQ-PE.

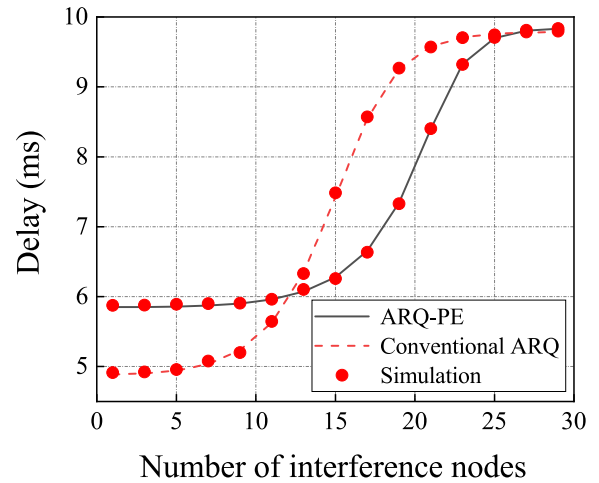


FIGURE 9. Delay versus the number of interference nodes for conventional ARQ and ARQ-PE.

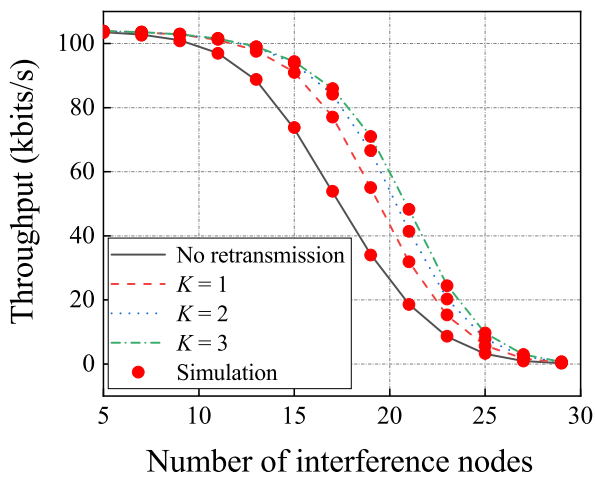


FIGURE 8. Throughput versus the number of interference nodes for ARQ-PE with different numbers of K .

to maximum throughput while still keeping K minimum for the advantage of delay or energy consumption. For example, as $n = 11$ we can set $K = 1$.

B. DELAY

Fig. 9 illustrates the delay versus the number of interference nodes of conventional ARQ and ARQ-PE. In this scenario, we set the packet arrival rate λ_{packet} by 0.05 and remove the limit of retransmissions to make the efficiency of ARQ-PE more clearly. ARQ-PE is more beneficial in terms of the delay time than the conventional ARQ. This is because each failed probing packet takes less time than the failed data packet. The delay is also an important aspect to consider in the setup of the network. For example, in sparse UWSNs ($n < 10$), ARQ-PE may take more delay due to the transmission of additional probing packets. But it is the appropriate protocol to reduce the delay in the harsh environment of dense UWSNs.

Fig. 10 represents the delay versus the number of interference nodes of ARQ-PE with different K . The setting of λ_{packet} in this scenario is as same as in Fig. 9. The figure proves that

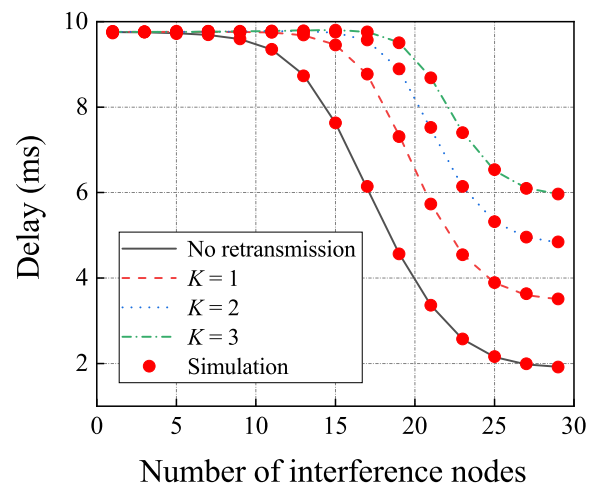


FIGURE 10. Delay versus the number of interference nodes for ARQ-PE with different numbers of K .

the larger number of retransmissions K , the greater the delay which the network conducts. For example, in the UWSNs with 25 interference nodes, the average delay is 2 ms when we transmit it only once. However, the delay is increased by 6 ms at $K = 3$. It also concludes that the number of retransmissions K affects the throughput and delay in two opposing tendencies: Fig. 8 above has shown that the throughput may be enhanced if K increases. This result is beneficial for choosing the optimal K in designing the network to maximize the throughput while minimizing the delay. However, we can consider this trade-off for multiple purposes when designing a specific network. For example, the UWSNs require low latency to reduce the number of retransmissions K as well as the throughput to achieve the right performance.

C. ENERGY EFFICIENCY

The relationship between energy efficiency and transmission power can be depicted in Fig. 11. As mentioned above,

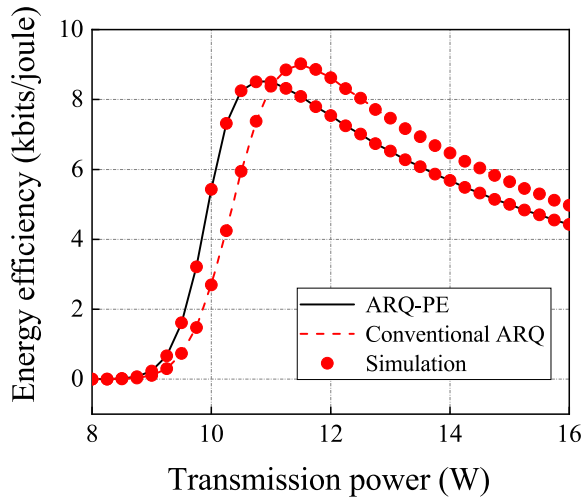


FIGURE 11. Energy efficiency versus transmission power for conventional ARQ and ARQ-PE.

the transmission power improves the signal power of the optical source, it however increases the energy cost of a data packet also. Therefore, it can be seen from the figure that the energy efficiency rises when the transmission power starts increasing. This is because the SINR of the optical link is enhanced, and the probability of transmitting a successful data packet is increased consequently. However, the energy efficiency declines at a certain point due to the overspending energy cost for a single data packet, which makes the sensor node deplete energy faster. The peak point, where the network uses energy most efficiently, can be defined as the optimal transmission power. Determining the optimal transmission power P_t to reach the maximum energy efficiency is necessary for transmitting packets reliably and saving energy in UWSNs. In this considered situation, optimal transmission powers of ARQ-PE and conventional ARQ are respectively 10.5 and 11.5 Watts.

One more thing can be conducted from Fig. 11 is that ARQ-PE is an ideal approach for low-power underwater sensors even though a probing packet always costs additional energy. It is because ARQ-PE takes less punishment of energy from a failed data packet sending, which helps the node reduce waste of energy and keep it in active mode for more retransmissions. The energy efficiency of ARQ-PE is better than that of conventional ARQ in the range of 8 to 11 Watts and vice versa when $P_t > 11$ Watts.

V. CONCLUSION

We have proposed a novel retransmission scheme based on probing packet and energy harvesting for improving the reliability and energy efficiency of the Internet of Underwater Things (IoUT) networks with Underwater Optical Wireless Communication (UOWC). A Markov chain model is proposed to analyze the network performance in terms of throughput, delay, and energy efficiency. The Monte-Carlo simulation confirms the correctness of the analytical model.

From the results, the proposed scheme is appeared to perform better than the traditional one for the dense and harsh network environment. We also optimize the operation of the proposed scheme by selecting the optimal number of retransmissions for a trade-off between throughput and delay. We believe that this study could be helpful for the pre-design of UOWC-based IoUT networks.

For future works, other retransmission schemes (e.g., Go-Back-N ARQ, and Selective Repeat ARQ) will be jointly considered with probing packets to further improve the network performance. Also, other issues on energy harvesting (e.g., energy overflow) and UOWC channel modeling (e.g., pointing errors and blockage) will be studied for a more comprehensive analysis.

REFERENCES

- [1] J. P. Espada, O. S. Martínez, J. M. C. Lovelle, B. C. P. G-Bustelo, M. Á. Álvarez, and A. G. García, "Modeling architecture for collaborative virtual objects based on services," *J. Netw. Comput. Appl.*, vol. 34, no. 5, pp. 1634–1647, Sep. 2011.
- [2] X. Zhang, J.-H. Cui, S. Das, M. Gerla, and M. Chitre, "Underwater wireless communications and networks: Theory and application: Part 1 [guest editorial]," *IEEE Commun. Mag.*, vol. 53, no. 11, pp. 40–41, Nov. 2015.
- [3] I. F. Akyildiz, D. Pompili, and T. Melodia, "Underwater acoustic sensor networks: Research challenges," *Ad Hoc Netw.*, vol. 3, no. 3, pp. 257–279, May 2005.
- [4] M. C. Domingo, "An overview of the Internet of underwater things," *J. Netw. Comput. Appl.*, vol. 35, no. 6, pp. 1879–1890, 2012.
- [5] G. Cossu, A. Sturmiolo, A. Messa, D. Scaradozzi, and E. Ciaramella, "Full-fledged 10base-t Ethernet underwater optical wireless communication system," *IEEE J. Sel. Areas Commun.*, vol. 36, no. 1, pp. 194–202, Jan. 2017.
- [6] M. Stojanovic and J. Preisig, "Underwater acoustic communication channels: Propagation models and statistical characterization," *IEEE Commun. Mag.*, vol. 47, no. 1, pp. 84–89, Jan. 2009.
- [7] I. F. Akyildiz, D. Pompili, and T. Melodia, "Challenges for efficient communication in underwater acoustic sensor networks," *ACM SIGBED Rev.*, vol. 1, no. 2, pp. 3–8, Jul. 2004.
- [8] X. Che, I. Wells, G. Dickers, P. Kear, and X. Gong, "Re-evaluation of RF electromagnetic communication in underwater sensor networks," *IEEE Commun. Mag.*, vol. 48, no. 12, pp. 143–151, Dec. 2010.
- [9] H. Kaushal and G. Kaddoum, "Underwater optical wireless communication," *IEEE Access*, vol. 4, no. 4, pp. 1518–1547, 2016.
- [10] C. D. Mobley, *Light and Water: Radiative Transfer in Natural Waters*. Cambridge, MA, USA: Academic, 1994.
- [11] J. S. Everett, "Forward-error correction coding for underwater free-space optical communication," Ph.D. dissertation, Dept. Elect. Eng., North Carolina State Univ., Raleigh, North Carolina, USA, 2009.
- [12] W. C. Cox, J. A. Simpson, C. P. Domizioli, J. F. Muth, and B. L. Hughes, "An underwater optical communication system implementing Reed–Solomon channel coding," in *Proc. OCEANS*, Quebec City, QC, Canada, Sep. 2008, pp. 1–6.
- [13] T. Shafique, O. Amin, M. Abdallah, I. S. Ansari, M.-S. Alouini, and K. Qaraqe, "Performance analysis of single-photon avalanche diode underwater VLC system using ARQ," *IEEE Photon. J.*, vol. 9, no. 5, pp. 1–11, Oct. 2017.
- [14] C. T. Nguyen, M. T. Nguyen, and V. V. Mai, "Underwater optical wireless communication-based IoUT networks: MAC performance analysis and improvement," *Opt. Switching Netw.*, vol. 37, May 2020, Art. no. 100570.
- [15] S. Sudevalayam and P. Kulkarni, "Energy harvesting sensor nodes: Survey and implications," *IEEE Commun. Surveys Tuts.*, vol. 13, no. 3, pp. 443–461, 3rd Quart., 2011.
- [16] N. Saeed, A. Celik, T. Y. Al-Naffouri, and M.-S. Alouini, "Localization of energy harvesting empowered underwater optical wireless sensor networks," *IEEE Trans. Wireless Commun.*, vol. 18, no. 5, pp. 2652–2663, May 2019.
- [17] H. H. Mahmoud, A. Hany, K. Fathy, and S. O. Abdelatif, "Throughput of underwater wireless sensor nodes with energy harvesting capabilities using RF and optical links," *Int. J. Electr. Electron. Eng. Telecommun.*, vol. 8, no. 3, pp. 177–180, 2019.

- [18] G. Baiden, Y. Bissiri, and A. Masoti, "Paving the way for a future underwater omni-directional wireless optical communication systems," *Ocean Eng.*, vol. 36, nos. 9–10, pp. 633–640, Jul. 2009.
- [19] D. Porcarelli, D. Brunelli, M. Magno, and L. Benini, "A multi-harvester architecture with hybrid storage devices and smart capabilities for low power systems," in *Proc. Int. Symp. Power Electron. Power Electron., Electr. Drives, Autom. Motion*, Jun. 2012, pp. 946–951.
- [20] M. Rahimnejad, A. Adhami, S. Darvari, A. Zirepour, and S.-E. Oh, "Microbial fuel cell as new technology for bioelectricity generation: A review," *Alexandria Eng. J.*, vol. 54, no. 3, pp. 745–756, Sep. 2015.
- [21] W.-Y. Chang, "The state of charge estimating methods for battery: A review," *ISRN Appl. Math.*, vol. 2013, pp. 1–7, Jul. 2013.
- [22] T. Komine and M. Nakagawa, "Fundamental analysis for visible-light communication system using LED lights," *IEEE Trans. Consum. Electron.*, vol. 50, no. 1, pp. 100–107, Feb. 2004.
- [23] S. Arnon and D. Kedar, "Non-line-of-sight underwater optical wireless communication network," *J. Opt. Soc. Amer. A, Opt. Image Sci.*, vol. 26, no. 3, pp. 530–539, 2009.
- [24] V. I. Haltrin, "Chlorophyll-based model of seawater optical properties," *Appl. Opt.*, vol. 38, no. 33, pp. 6826–6832, 1999.
- [25] R. O. Blanco and R. M. de Moraes, "Signal-to-noise and interference ratio analysis for ALOHA underwater acoustic networks," in *Proc. Int. Workshop Telecommun. (IWT)*, Jun. 2015, pp. 1–6.
- [26] P. Billingsley, *Probability and Measure*. Hoboken, NJ, USA: Wiley, 2008.
- [27] M. T. Nguyen, V. V. Mai, and C. T. Nguyen, "SINR performance analysis of 3-D underwater optical wireless communication networks," in *Proc. 26th Int. Conf. Telecommun. (ICT)*, Ha Noi, Viet Nam, Apr. 2019, pp. 41–45.
- [28] M. V. Jamali, A. Mirani, A. Parsay, B. Abolhassani, P. Nabavi, A. Chizari, P. Khorramshahi, S. Abdollahramezani, and J. A. Salehi, "Statistical studies of fading in underwater wireless optical channels in the presence of air bubble, temperature, and salinity random variations," *IEEE Trans. Commun.*, vol. 66, no. 10, pp. 4706–4723, May 2018.
- [29] R. Barrios and F. Dios, "Exponentiated weibull fading channel model in free-space optical communications under atmospheric turbulence," Ph.D. dissertation, Dept. Signal Theory Commun., Polytechnic Univ. Catalonia, Barcelona, Spain, Apr. 2013.
- [30] M. A. Berger, "Markov chains—Stationary distributions and steady state," in *An Introduction to Probability and Stochastic Processes*. New York, NY, USA: Springer, 1993, pp. 101–120.
- [31] M. Doniec, C. Detweiler, I. Vasilescu, M. Chitre, M. Hoffmann-Kuhnt, and D. Rus, "AquaOptical: A lightweight device for high-rate long-range underwater point-to-point communication," *Mar. Technol. Soc. J.*, vol. 44, no. 4, pp. 55–65, Jul. 2010.



CUONG T. NGUYEN is currently pursuing the bachelor's degree in communications engineering with the Hanoi University of Science and Technology (HUST). He is also working as a Research Assistant with the Communications Theory and Applications Research Group (CTARG), School of Electronics and Telecommunications, HUST. His research interest includes reliable transmission in optical wireless networks.



VUONG V. MAI (Member, IEEE) received the M.S. and Ph.D. degrees in computer science and engineering from The University of Aizu, Japan, in 2014 and 2017, respectively. He joined the Korea Advanced Institute of Science and Technology (KAIST), South Korea, as a Postdoctoral Fellow, in April 2017, where he is currently a Research Assistant Professor with the School of Electrical Engineering. His current research interest includes optical wireless technologies and applications.



CHUYEN T. NGUYEN received the B.E. degree in electronics and telecommunications from the Hanoi University of Science and Technology (HUST), Vietnam, in 2006, the M.S. degree in communications engineering from National Tsing Hua University, Taiwan, in 2008, and the Ph.D. degree in informatics from Kyoto University, Japan, in 2013. From September to November 2014, he was a Visiting Researcher with The University of Aizu, Japan. He is currently an Associate Professor with the School of Electronics and Telecommunications, HUST. His current research interests include MAC protocol design and reliable transmission in wireless/optical networks. He received the Fellow Award from the Hitachi Global Foundation in August 2016.

• • •